Chalcogenide Letters Vol. 22, No. 8, August 2025, p. 679 - 691

Sonochemically synthesised nitrogen-doped CdS nanoparticles for photovoltaic applications

S. R. Ahmed [a *], M. V. V. K. Srinivas Prasad [b], K. Keerthivasan [c]
[a] *Department of Physics, Koneru Lakshmaiah Education Foundation, Green Fields, Vaddeswaram, Guntur District, A.P, PIN CODE: 522502, India.*
[b] *Department of Physics, Koneru Lakshmaiah Education Foundation, Green Fields, Vaddeswaram, Guntur District, A.P, PIN CODE: 522502, India.*
[c] *Department of Electrical Engineering, University of Technology and Applied Sciences PO Box 74. AlKhuwair, Muscat Sultanate of Oman.*

This work used a sonication-aided approach to make Cadmium sulfide nanoparticles and Nitrogen-doped CdS nanoparticles. Doping Nitrogen into CdS NPs enhances the material's electrical, chemical, and structural properties by altering its surface area and functional sites. XRD, FTIR, SEM/EDX, TGA, UV-Vis, and PSA are used to evaluate the characteristic features of CdS NPs. The photovoltaic responses of the prepared CdS and CdS-N NPs were evaluated by electrochemical impedance and IV analysis. The obtained XRD data confirms that nitrogen doping significantly changes the crystal size of CdS NPs. The XPS spectrum depicts the presence of trace elements and confirms the nitrogen doping with CdS. The absorption spectra and band gap values derived from UV data demonstrate that nitrogen doping improves the optical characteristics of CdS NPs in the long run. CdS thin film photoanodes show improved photoresponse, even at such low bias voltages, according to the electrical characterisations.

(Received December 28, 2024; Accepted August 5, 2025)

Keywords: Cadmium sulfide N.P.s, Nitrogen-doped CdS, XPS analysis, Solar cell applications

1. Introduction

In the last few decades, researchers have focused on semiconductor nanocrystals' electrical and structural features. The size-dependent optical characteristic in the zone where the nanocrystal is smaller than the bulk excitons drive the continued interest in this material class. Quantum confinement of the charge carriers produces a blue shift of the absorption onset of up to 1 eV and the emergence of distinct characteristics in the optical spectra as the nanocrystal size decreases [1, 2]. Nanoparticles (NPs), semiconductor nanomaterials, have been extensively explored for their future optoelectronic applications [3, 4]. Due to their distinct and unique characteristics, such as excellent light-harvesting capacity, enormous surface area, variable optical and electrical characteristics, and exceptional photostability, semiconductor nanoparticles (NPs) have recently become the most advanced nanostructured materials for photocatalytic applications. NPs band gaps vary depending on nanocrystal size, allowing for variations in absorption rates even when employing the same absorber material [5, 6]. This property is beneficial for increasing the light absorption range of quantum dot semiconductor nanostructures [7]. In particular, NPs may absorb several photons simultaneously, even after electrons and holes have accumulated, indicating that they could be used in the highly functional photon-to-electron conversion [8].

Furthermore, by doping, plating, combining with shells, or capping with functional groups, the physiochemical characteristics of NPs can be easily modified [9-11]. Impurity doping is a practical approach for changing semiconductors' electrical and physicochemical properties. Impurity concentrations underneath the conduction band (CB) have been discovered in metal dopants, which behave as photo-induced electron entrapment sites. The CdS nanoparticles (NPs)

* Corresponding author: rafeeksra@gmail.com
https://doi.org/10.15251/CL.2025.228.679

are a popular form of II-IV nanomaterial that plays a significant role in core-shell NPs due to their significant bandgap energy [12]. As the synthesis of discrete and enhanced high-quality NPs has progressed, CdS NPs have a more significant potential [13]. CdS nanoparticles are also a predominant material for applications in biology, gas sensors, and solar cells [14-17].

In the present work, two samples were prepared. The first sample is cadmium sulfide nanoparticles (CdS) prepared using a sonication-aided technique, while the second sample is cadmium sulfide nanoparticles with nitrogen doping (CdS-N). Doping Nitrogen in CdS NPs is to progress the material's electrical, chemical, and structural characteristics by modifying its surface area and functional sites [18-20]. As per the literature survey, urea's structural, morphological and optical properties could be highly enhanced as nitrogen doping sources compared with other sources like ammonia, melamine, glycine, etc., [20]. XRD, SEM, and FTIR were used to examine the prepared samples' morphological and structural properties. The example's optical properties were concentrated on utilising UV and PL. The photovoltaic responses of the prepared CdS and CdS-N NPs are evaluated in the form of CdS thin films as photoanodes.

2. Experimental

2.1. Materials

Cadmium chloride, Sodium Sulphide Flakes, citric acid, and Urea were purchased from Merck. Apart from these materials, double distilled water and Whatman No. 1 filter papers were used to prepare CdS and nitrogen-doped CdS NPs.

2.2. Method

0.001 M of Cadmium chloride solution, 0.002 M of citric acid, and 0.001 M Sodium Sulphide Flakes solutions were prepared separately. Drop by drop, citric acid was added to the cadmium chloride solution, which was then agitated for 30 minutes to create a homogeneous solution. After that, sodium sulfite solution was added to the above solution, which resulted in a yellow colour solution that indicates the CdS formation and the final solution was stirred for 4 hours to enhance the reaction. The above mixture was stimulated using a magnetic stirrer for 24 h at room temperature and sonicated for 60 mins. The obtained orange-yellow CdS was centrifuged, rinsed with DDW, and then dried for 4 hours at 110 °C. Hereafter, the collected sample will be named CdS. To synthesise the N-doped CdS, 1M of Urea powders was added to the cadmium chloride and sodium sulfate solution, and the other procedures were the same as like CdS synthesis procedure. The Nitrogen-doped CdS sample is called CdS-N NPs.

2.3. Preparation of CdS and CdS-N thin films for IV measurements

We measured the IV using a Newport solar simulator (model 91160) with an AM 1.5 G spectrum supply and a Keithley 2400 source meter. As anodes, DSSC cells utilised CdS-N thin films. Furthermore, the CdS and CdS-N NPs were all weighed independently, trailed by the expansion of Acetyl $(CH_3)_2CO$ and two drops of Criton X-100, and the blend was consistently joined with a mortar until slurry was framed. Scotch Magic tape was used to cut a 1 cm^2 window that adhered to the conductive side of the ITO glass. A mixture of CdS and CdS-N NPs filled the ITO glass. At 150 degrees Celsius, this procedure takes about 60 minutes. After twelve hours of submerging the samples in Ruthenium N71 dye, we constructed the cell with an electrode coated in platinum and a liquid lithium iodide as the electrolyte.

2.4. Characterisation of CdS and CdS-N nanoparticles

XRD instrument (Rigaku Ultima IV) was used to assess the phases of CdS and CdS-N. FullProf analytical software was used to perform Rietveld analysis on the prepared samples. A Fourier transform infrared spectroscopy (FTIR) (Spectrum 100; PerkinElmer, USA) was used to investigate the functional groups. The thermal longevity of the samples is investigated using a Thermogravimetric analyser (Perkin – Elmer STA 5000). X-ray photoelectron spectroscopy (XPS) analyses were performed using a K-Alpha Thermo Scientific spectrometer to confirm the doping and presence of Cd, S and N. Using a particle size analyser (Shimadzu ZT 1700), the average

particle size was investigated. The absorbance of the prepared samples is measured using UV-Vis spectroscopy (Shimadzu, UV-2700i)

3. Results and discussion

3.1. Structural analysis

Figure 1 illustrates the XRD results of CdS NPs. The prominent peaks are 24.810, 26.520, 28.200, 36.650, 43.660, 48.010, and 51.830. The peaks mentioned above line up with the crystal plane (100), (002), (101), (102), (110), (103), and (112), respectively. The detected peaks correlate with the JCPDS Card number 41-1049 and index to a hexagonal crystal structure with space group P63mc (186) [21]. The more substantial peaks clearly show that the produced samples have high crystallinity. The results showed fewer noises, indicating that the samples prepared were impurity-free.

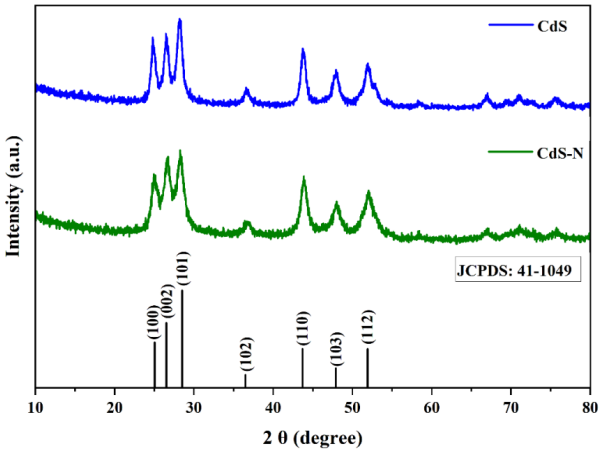

Fig. 1 XRD analysis of CdS and CdS-N NPs.

The crystal size was calculated using the debye Scherer equation and tabulated in Table 1 [17, 18]. The calculated mean crystal size of prepared CdS and CdS-N is 12.65 nm and 13.22 nm, respectively.

Table 1. Mean crystal size obtained from XRD data of CdS and CdS-N NPs.

(*hkl*)	FWHM (degree)		2 θ (degrees)	Crystal size (nm)	
	CdS	CdS-N		CdS	CdS-N
(100)	0.6602	0.4684	24.96	12.31	14.31
(002)	0.6353	0.6022	26.64	12.84	13.55
(101)	0.6453	0.6691	28.04	12.68	12.24
(102)	0.6691	0.6691	43.80	12.78	12.79
			Average crystal size	12.65	13.22

The resulting CdS samples were refined using the Pseudo Voigt function [22, 23]. The revised graphs of CdS and CdS-N are presented in Figure 2. Where the sample's estimated crystal structure and other corrected data are shown in Table 2. The R factors discovered in the refinement data match previously found [24].

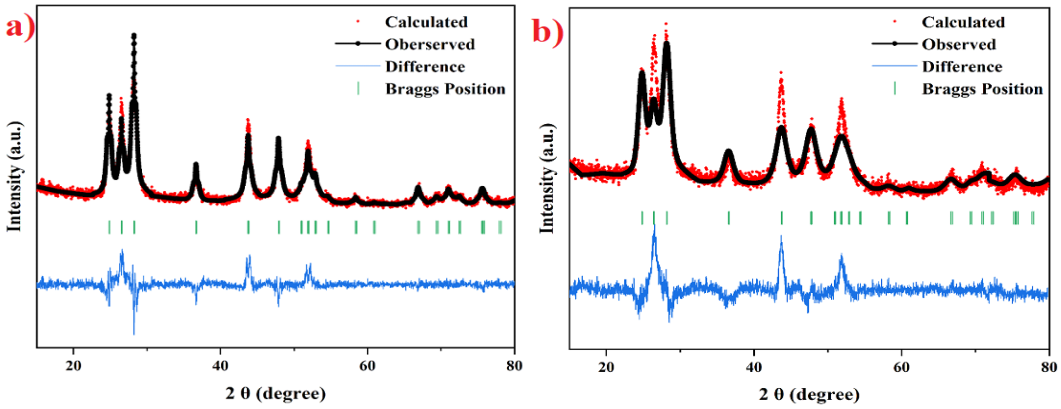

Fig. 2. Rietveld refinements of CdS and CdS-N NPs.

Table 2. Refined parameters of CdS and CdS-N NPs.

Space group: P63mc (186) (Hexagonal)							
Sample	**a =b (Å)**	**c (Å)**	**Volume (Å)**	**R_p**	**R_{wp}**	**R_{exp}**	**χ^2**
CdS	4.135	6.71	99.49	10.6	13.5	9.94	1.8
CdS-N	4.140	6.746	100.13	11.5	14.8	9.93	2.21

3.2. Thermal stability analysis

Figure 3 depicts the investigation of the thermal stability of CdS NPs. The initial step of decomposition of a CdS sample results in a 13.5 % weight loss at temperatures ranging from 800 to 4500 C, wherein absorbed water molecules and other physically associated molecules are disintegrated. In the range of 4700 - 7800 C, the second stage of decomposition occurs at 22.8 %, and the complete breakdown rate of produced CdS is 43.1 %. Similarly, 8.7% of weight loss happens between 80 and 450 °C, and 11.3 % occurs between 470 and 780 0C, resulting in a total weight loss of 24 % in CdS-N NPs. The TGA results show that the significant nitrogen bond formation caused in the CdS-N sample leads to more excellent thermal stability than the undoped CdS sample [25].

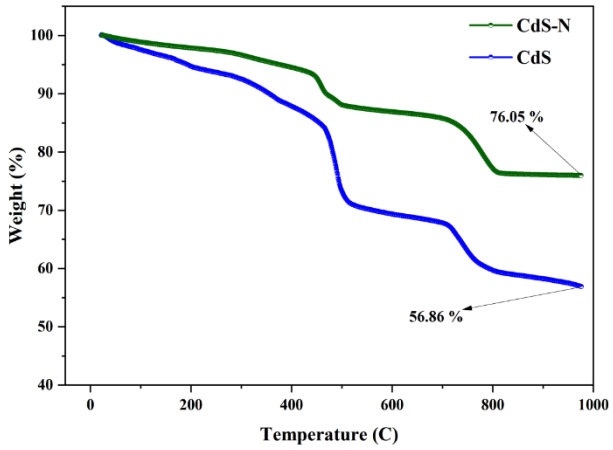

Fig. 3. Thermo gravimetric analyses of CdS and CdS-N NPs.

3.3. Functional analysis

The functional analysis of CdS NPs is represented in Figure 4(a) and (b), respectively. The peak obtained at 3405 cm-1 falls under the wavelength range of 3500-3000 cm^{-1}, which may occur due to the stretching vibration of O-H and H-O-H bonds [26]. This is due to the moisture absorption of the sample or KBr. Sharp peaks in the region 3000-3250 cm^{-1} represent the bond stretching of γ-Cd $(OH)_2$ [27]. The sharp peaks observed in the region of 1643 and 1406 cm^{-1} wavelength are owing to the stretching of C=O and C-H bonds. The peaks observed in the 670 to 720 cm^{-1} represent the CdS stretching [28]. Eventually, we obtained a sharp peak at 679 cm^{-1} resulting in the bond stretching of CdS. In Figure 3, the CdS-N NPs FTIR spectrum (b) attains a peak at 1046 cm^{-1}, resulting in the stretching of the doped Nitrogen compound as a C-N bond [29].

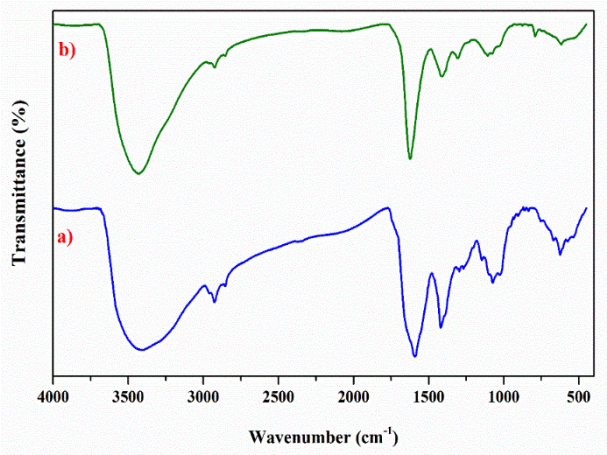

Fig. 4. FTIR spectra of CdS and CdS-N NPs.

3.4. Particle size analysis

The mean particle size of the samples is displayed in Figure 5. The obtained mean particle size of CdS NPs are 16.7 nm (d_{50}) and 18.65 nm (d_{50}), respectively. The size of CdS ranges from 5 nm (d_{10}) to 40 nm (d_{90}). Similarly, for CdS-N, the particle size ranges from 6 nm (d_{10}) to 45 nm (d_{90}). As a result of the particle sizes achieved for CdS and CdS-N, the prepared sample is obviously in the nanoscale. When comparing the particle sizes of the two samples, the particle size of CdS-N seems to be significantly larger owing to nitrogen doping [30].

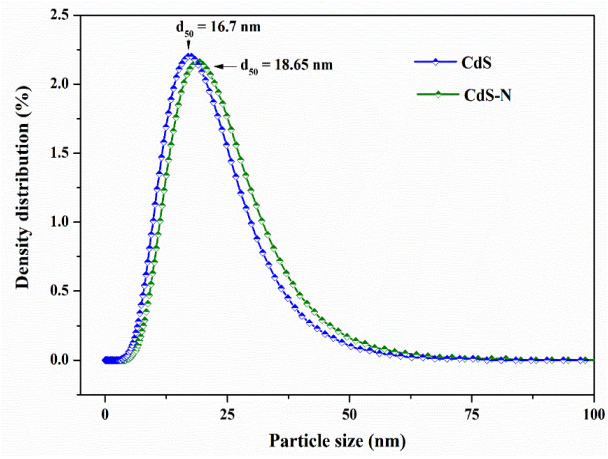

Fig. 5. Average particle size distributions of CdS and CdS-N NPs.

3.5. Morphological analysis

The SEM images of CdS are shown in Figure 6. For CdS nanoparticles, the samples demonstrate layered planar sheet growth. In addition, the particles looked like a regular and uniform shape. As observed in SEM pictures, the average particle size of the CdS and CdS-N nanoparticles is petite, as validated by XRD and particle size analyses. The EDX analysis of CdS-N samples was performed to verify the Nitrogen content and composition of CdS and CdS-N samples. EDX spectra of CdS and CdS-N are shown in Figures 3 (b and d). A table of the elemental distributions of the prepared samples is shown in the inset. The prepared CdS and CdS-N samples show uniform distributions. It can be seen from the EDX spectra that not only are Cd, S, and N present in the CdS-N matrix but they are distributed uniformly within its matrix.

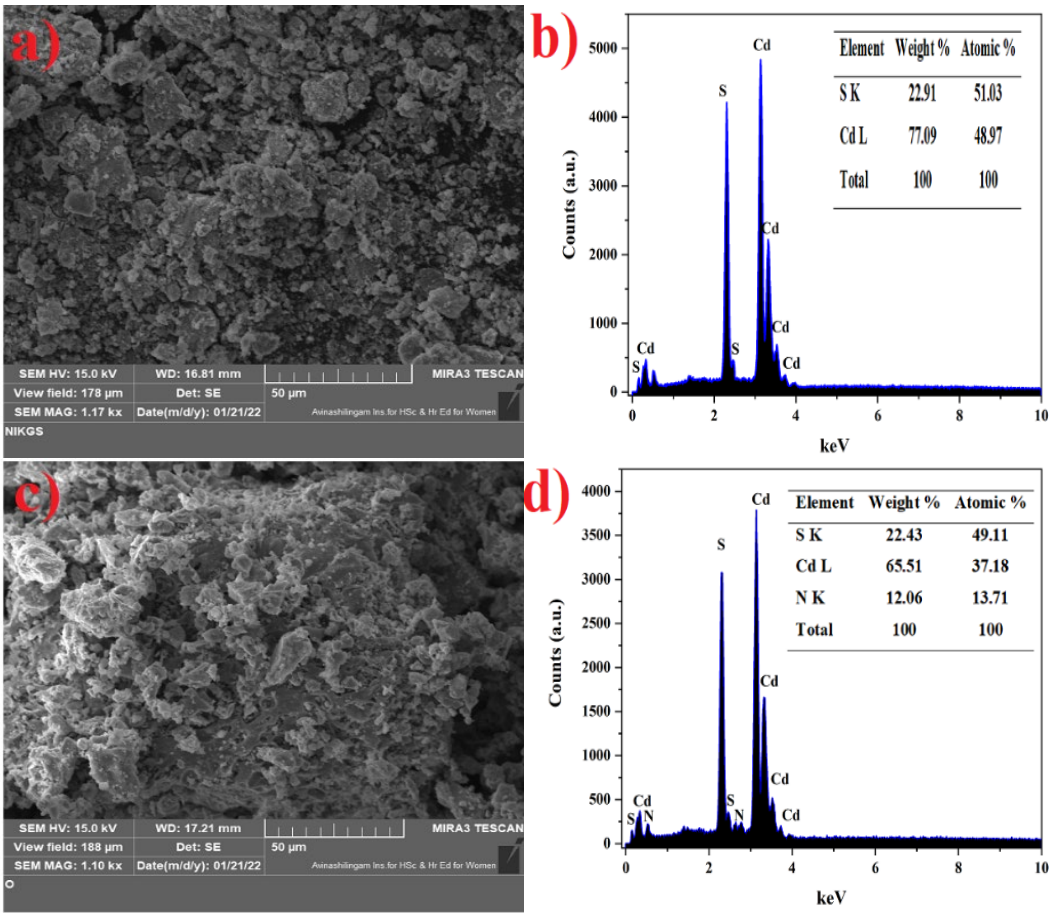

Fig. 6. SEM images and EDAX spectra of CdS and CdS-N NPs.

Figure 7 depicts the outcomes, which include the CdS and CdS-N nanoparticle SAED and HRTEM patterns. The low-magnification CdS and CdS-N nanoparticles indicate that the samples with the SAED in Figure 7(b) and (d) are agglomerated nanoparticles. According to the d-values of the diffraction rings in both samples, which are consistent with the results of XRD analyses, the cubic modification is the predominant one in both CdS and CdS-N nanoparticles. The samples are vastly different from one another. In addition to the diffuse rings, the CdS-N nanoparticles' SAED pattern contains more reflection dots, indicating the presence of nanoparticles slightly more prominent than those smaller than them. CdS nanoparticles, on the other hand, have diffuse diffraction rings that show that they are made up of tiny nanoparticles with an average size of nearly 10 nm. Consequently, the HRTEM and SAED patterns made it abundantly clear that the addition of nitrogen ions to CdS nanoparticles ought to result in modifications to their size and morphology.

3.6. XPS analysis

Fig. 8 displays the XPS analysis findings. According to XPS analyses, traces of the reactants, including carbon and oxygen from organic compounds that might be absorbed in the surface of the fine powders during processing, were found in the processed CdS-N nanoparticles. The XPS survey spectrum is shown in Fig. 8, and it contains peaks from Cd, S, O, and N. The XPS spectra of Cd 3d having peaks at 401 and 408 eV, which correspond to Cd 3d3/2 and Cd 3d5/2, respectively, are shown in Fig. 7(b). The peaks at 156.5 and 157.8 eV in the S 2p XPS spectra shown in Fig. 8(c) correspond to S 2p3/2 and S 2p1/2, respectively. The CdS-N nanoparticles' surface material oxidises from exposure to air and the presence of surface impurities, which causes photo-corrosion of the surface material. The peaks of O 1s and C 1s at 281.5 and 529.15 eV, respectively, are probably caused by contaminants that have been adsorbed. Figure 8 (d) shows the N 1s region's XPS spectrum. The interstitial nitrogen bound to the lattice oxygen was attributed to the peak positions of N 1s at 401.21 and 408.51 eV. Last but not least, it shows that the nitrogenisation of the samples was successful.

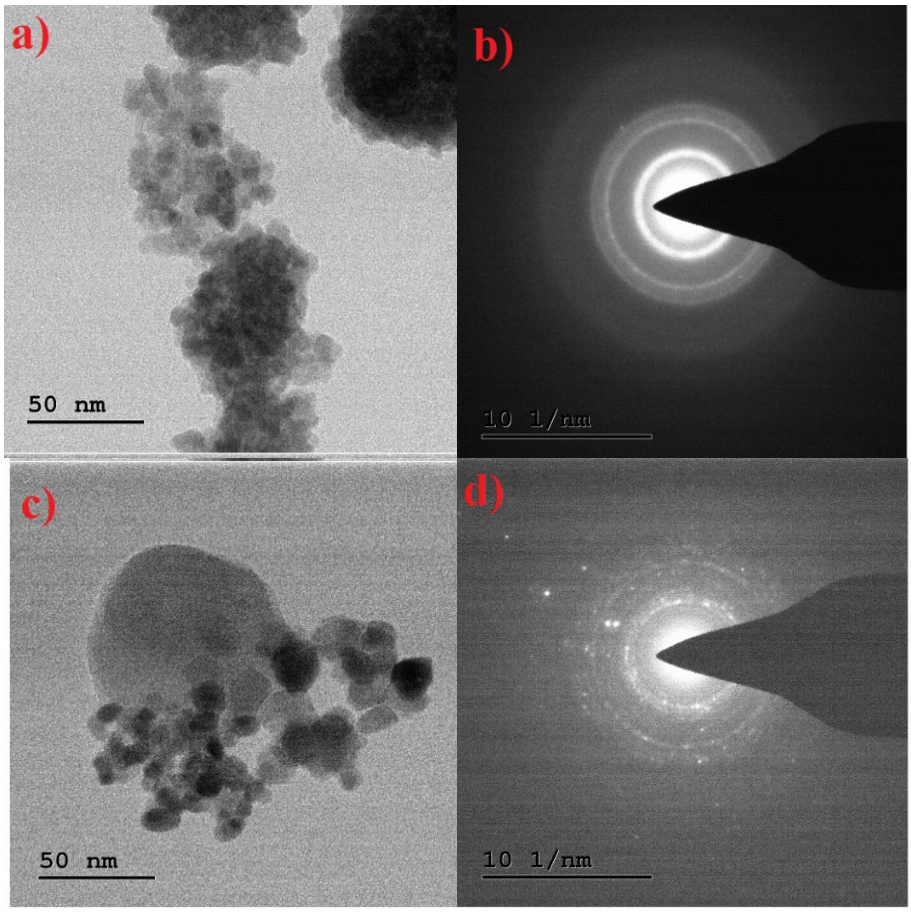

Fig. 7. HRTEM images (a and c) and SAED patterns (c and d) of CdS and CdS-N nanoparticles.

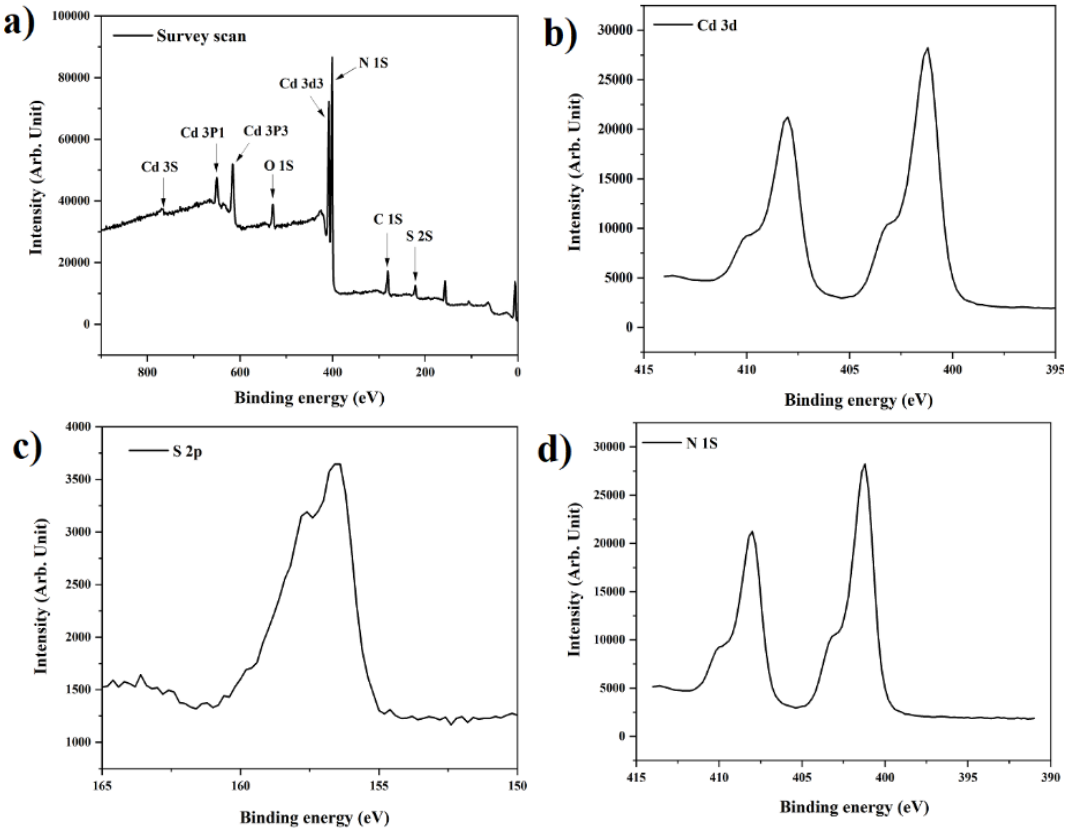

Fig. 8. XPS spectra of the CdS-N nanoparticles, (a) Survey scan, (b) Cd 3d, (c) S 2P, (d) N 1S.

3.7. Optical analysis

The UV-Vis absorption spectra of the prepared sample are illustrated in Figure 9a. CdS and CdS-N absorption spectra exhibit a wide shoulder with a trace toward higher wavelengths. Undoped CdS has a sharp peak in the 280-300 nm region, whereas CdS-N has a broader sharp peak in the 300-320 nm range. As a result, the absorption range of CdS-N is in the higher wavelength range. Figure 9(b) shows the transmittance percent of the prepared samples, which shows that transmittance rises linearly with wavelength. As seen in the transmittance graph, the sample's optical transmittance is eventually induced by nitrogen doping [31, 32].

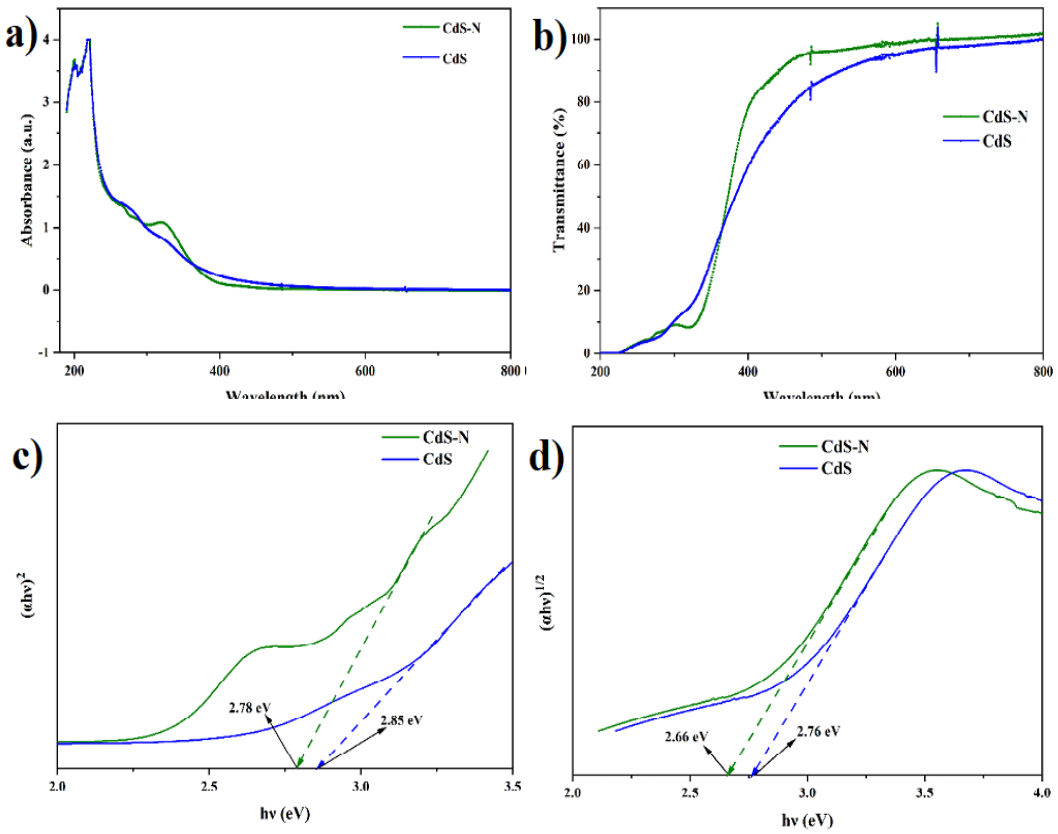

Fig. 9. a) Absorption spectra obtained from UV-Vis b) Transmittance spectra c) Direct bandgap calculated using Tauc plot d) Indirect bandgap obtained using Tauc plot of CdS and CdS-N NPs.

The direct and indirect band gaps of synthesised samples are displayed in Figures 9c and 7d, respectively. The bandgap of the material is calculated using the Tauc equation [33]. The quantum confinement phenomenon, connected to particle size, is responsible for the blue shift absorption spectra discovered. Due to the quantum confinement effect, a nanoparticle's bandgap increases as the particle's size decreases, causing absorption spectra to shift to a lower wavelength [34]. CdS has a direct bandgap of 2.85 eV, while CdS-N has 2.78 eV. The indirect bandgap of CdS and CdS-N are 2.76 and 2.66 eV, respectively. According to the obtained bandgap, nitrogen doping spans a broad frequency range, resulting in a smaller bandgap [35].

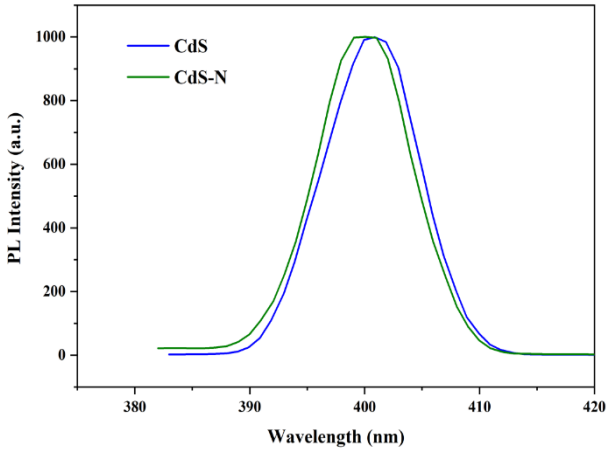

Fig. 10. PL Spectra of CdS and CdS-N NPs.

Figure 10 shows the standardised PL spectra of the CdS nanoparticles excited at 382 nm. It shows that pure and Nitrogen-doped CdS NPs exhibit a strong PL peak at about 400 nm. Also, PL peaks can be observed shifting towards lower wavelength. The excitons transitions could be responsible for the 398 and 400 nm PL peak. Doping the Nitrogen to CdS NPs favours this tendency [36-38].

3.8. Electrochemical studies

In Figure 11, you can see the Nyquist plots of CdS and CdS-N thin films. There are semicircles in both of them near the high-frequency region. The arc indicates how much resistance the electrode has to transfer charge. The high Rct of thin film electrodes made from CdS is more remarkable than those made from CdS-N; this indicates that the sensitising CdS-N significantly improves the charge transfer characteristics of the photoanode/electrolyte interface. However, the diameter of the semicircle of the CdS-N thin film is larger than the diameter of the CdS thin film sample, which indicates that sensitising CdS-N thin film can prolong charge carriers' lifetimes, incorporating this into a solar cell's durability and enhancing its power conversion efficiency [39-43].

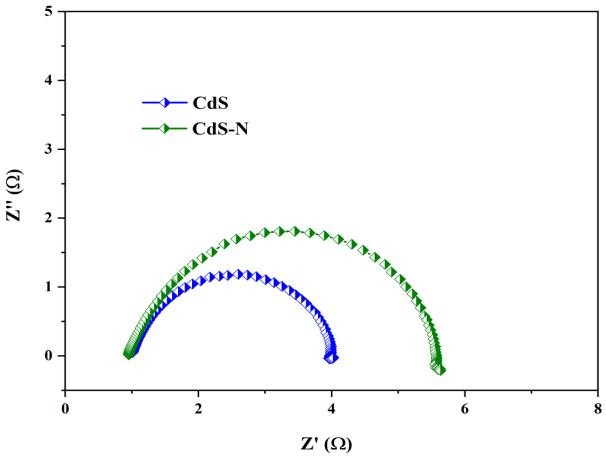

Fig. 11. Electrochemical impedance spectra of CdS and CdS-N thin films.

3.9. Photocurrent voltage characteristics

The photovoltaic characteristics parameters (Voc, Jsc, FF, and η) for CdS and CdS-N thin films are listed in Table 3. It is evident that the value of Jsc, Voc, and η rise as nitrogen is added to CdS NPs. This outcome may have been caused by the CdS-N thin films' highly rough and porous surface, which improved the optical absorption of the thin films [44]. Moreover, because of their excellent electrical conductivity, nitrogen ions could serve as bridges to speed up the transport of electrons from thin-film surfaces to the ITO plate electrode, potentially lowering electron-hole recombination rates. Further, nitrogen-doped CdS with a tiny structure can absorb more photons, creating an electronic transport tunnel and reducing the transmission path. S for photoanodes based on CdS-N thin films is more significant than that for photoanodes based on CdS thin films. This finding demonstrates that the incorporation of Nitrogen into CdS serves as a blocking layer to prevent back electron-hole recombination, increasing the effectiveness of energy conversion of photoanode. [45-49].

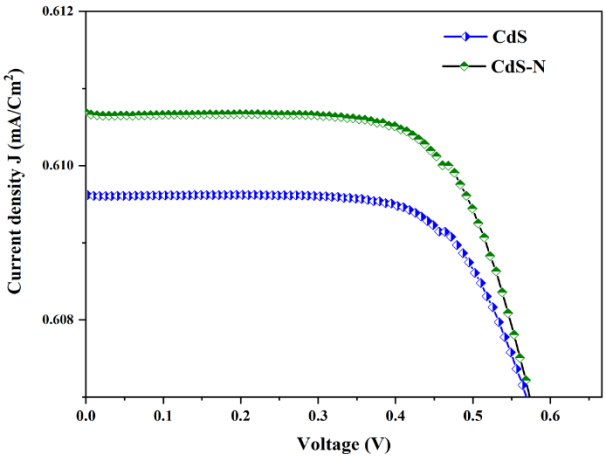

Fig. 12. Photocurrent-voltage characteristic plots of CdS and CdS-N thin films.

Table 3. Photovoltaic parameters of CdS and CdS-N thin films.

Sample	V_{oc} (V)	J_{sc} (mA/Cm^2)	V_{oc} * J_{sc}	V_{mp} (V)	J_{mp} (mA/Cm^2)	V_{max} * J_{max}	Fill factor	Efficiency η (%)
CdS	0.560	0.60	0.341	0.438	0.609	0.2667	0.63	2.14
CdS-N	0.579	0.61	0.353	0.418	0.610	0.2549	0.81	2.58

4. Conclusion

In conclusion, we have effectively synthesised CdS and CdS nanoparticles doped with nitrogen. Nitrogen doping impacted optical, morphological, and functional properties, which XRD, UV, FTIR, and SEM validated. The average particle size of CdS and CdS-N NPs are 16.7 nm and 18.65 nm, respectively, indicating that nitrogen doping over CdS NPs resulted in a significant shift in average size. CdS-N NPs have a smaller optical bandgap than undoped CdS, implying that CdS-N has more robust optoelectrical capabilities. Thermo gravimetric analysis confirms that nitrogen doping in CdS-N has a more significant effect on lowering the sample deterioration. Overall, the evidence shows that nitrogen doping in CdS NPs significantly impacts optoelectronic characteristics and has multi-function applications. The current-voltage (I-V) characterisation of the prepared thin film photoanode shows that the prepared CdS and CdS-N samples are possible candidates for a solar cell device. The light energy conversion efficiency based on CdS and CdS-N thin film samples is 1.854 and 2.485, respectively. It shows that the prepared CdS thin film solar cell performances can be improved by doping the nitrogen with it.

References

[1] J.W. Shi, D. Sun, Y. Zou, D. Ma, C. He, X. Ji, C. Niu, J. Chem. Eng 364: 11-19 (2019); https://doi.org/10.1016/j.cej.2019.01.147

[2] V. Kavitha, M. Jeyanthinath, P. Mahalingam, N. Sethupathi, Mater. Today-Proc. 35: 48-52 (2021); https://doi.org/10.1016/j.matpr.2019.05.437

[3] A.M. Smith, S. Nie, Acc. Chem. Res. 43: 190-200 (2009); https://doi.org/10.1021/ar9001069

[4] K. Kandasamy, S. Surendhiran, R. Chithra Devi, Y.A. Syed Khadar, P. Rajasingh, A. Balamurugan, AIP Conf. Proc. 2385, 020001 (2022); https://doi.org/10.1063/5.0070727

[5] Z.J. Li, J.J. Wang, X.B. Li, X.B. Fan, Q.Y. Meng, K. Feng, B. Chen, C.H. Tung, L.Z. Wu, Adv. Mater. 25: 6613-6618 (2013); https://doi.org/10.1002/adma.201302908

[6] MC Beard, J. Phys. Chem. Lett. 2: 1282-1288 (2011); https://doi.org/10.1021/jz200166y

[7] V. Kavitha, P. Mahalingam, M. Jeyanthinath, N. Sethupathi, Mater. Today-Proc. 23: 12-15 (2020); https://doi.org/10.1016/j.matpr.2019.05.351

[8] C. N. Omprakash Anand, P. Thirunavukkarasu, S. Surendhiran, K. C. Suresh, A. Balamurugan, Y. A. Syed Khadar, AIP Conf. Proc. 2385, 020006 (2022); https://doi.org/10.1063/5.0070918

[9] S Karthikeyan, K Dhanakodi, K Shanmugasundaram, S Surendhiran, Mater. Today: Proc. 47(4) 901-906 (2021); https://doi.org/10.1016/j.matpr.2021.04.473

[10] S. Ravikumar, S. Surendhiran, J. Sunil, K. C Suresh, A. Balamurugan, Y. A. Syed Khadar, A. Benham, AIP Conf. Proc. 2385, 020008 (2022); https://doi.org/10.1063/5.0070812

[11] H. Zhu, N. Song, H. Lv, CL Hill, T. Lian, J. Am.Chem. Soc. 134: 11701-11708 (2012); https://doi.org/10.1021/ja303698e

[12] M.A. Holmes, T.K. Townsend, F.E. Osterloh, Chem. Commun. 48: 371-373 (2012); https://doi.org/10.1039/C1CC16082F

[13] J.C. Wu, J. Zheng, P. Wu, R. Xu, J. Phys. Chem. C. 115: 5675-5682 (2011); https://doi.org/10.1021/jp109567c

[14] Y. Zou, J.W. Shi, D. Ma, Z. Fan, L. Cheng, D. Sun, Z. Wang, C. Niu, ChemSusChem. 11: 1187-1197 (2018); https://doi.org/10.1002/cssc.201800053

[15] K. Kandasamy, S. Surendhiran, Y.A. Syed Khadar, P. Rajasingh,
Mater. Today: Proc. 47 (3):757-762 (2021); https://doi.org/10.1016/j.matpr.2020.07.080

[16] Yu-Jen Shen, Yuh-Lang Lee. Nanotechnology. 19: 045602 (2008); https://doi.org/10.1088/0957-4484/19/04/045602

[17] Y.A. Syed Khadar, S. Surendhiran, V. Gowthambabu, S Halimabi Alias Shakila Banu, V. Devabharathi, A. Balamurugan, Today: Proc. 47(4) 889-893, (2021); https://doi.org/10.1016/j.matpr.2021.04.335

[18] V. Ha Chu, Thi Ha Lien Nghiem, T. Ha Le, D. Lam Vu, H. Nhung Tran, Thi Kim Lien Vu, Adv. Nat. Sci.: Nanosci. Nanotechnol. 3: 025017 (2012); https://doi.org/10.1088/2043-6262/3/2/025017

[19] H. Huang, B. Dai, W. Wang, C. Lu, J. Kou, Y. Ni, L. Wang, Z. Xu, Nano Lett. 17: 3803-3808 (2017); https://doi.org/10.1021/acs.nanolett.7b01147

[20] Q. Shen, Z. Jiang, X. Tian, H. Zhu, Z. Jiang, J. Alloys Compd. 884: 161073 (2021); https://doi.org/10.1016/j.jallcom.2021.161073

[21] M. Sudha, S. Surendhiran, V. Gowthambabu, A. Balamurugan, R. Anandarasu, Y.A. Syed Khadar, D. Vasudevan, J Bio Tribo Corros. 7:60 (2021); https://doi.org/10.1007/s40735-021-00492-w

[22] S. Karthikeyan, P. Thirunavukkarasu, S. Surendhiran, Y.A. Syed Khadar, A. Balamurugan, B. Gobinath, Mater. Today: Proc. 47(4) 970-977 (2021); https://doi.org/10.1016/j.matpr.2021.05.217

[23] S. Surendhiran, V. Gowthambabu, A. Balamurugan, M. Sudha, V.B. Senthil Kumar, K.C Suresh, Mater. Today: Proc. 47(4) 1011-1016 (2021); https://doi.org/10.1016/j.matpr.2021.05.515

[24] K.C. Suresh, S. Surendhiran, P. Manoj Kumar, E. Ranjith Kumar, Y.A. Syed Khadar, A. Balamurugan, SN Appl. Sci. 2:1735 (2020); https://doi.org/10.1007/s42452-020-03534-z

[25] Juan Rodriguez-Carvajal, Thierry Roisnel.FullProf.98 and WinPLOTR: New Windows 95/NT Applications for Diffraction Commission for Powder Diffraction, International Union for Crystallography, Newletter N°20 (1998).

[26] T. Roisnel, J. Rodriguez-Carvajal. WinPLOTR: a Windows tool for powder diffraction patterns analysis Materials Science Forum, Proceedings of the Seventh European Powder Diffraction Conference (EPDIC 7), (2000), p.118-123, Ed. R. Delhez and E.J. Mittenmeijer; https://doi.org/10.4028/www.scientific.net/MSF.378-381.118

[27] D. Vasudevan, D. Senthilkumar, S. Surendhiran, Int J Thermophys. 41:1-19 (2020); https://doi.org/10.1007/s10765-020-02651-6

[28] S. Sandoval, N. Kumar, A. Sundaresan, C.N.R. Rao, A. Fuertes, G. Tobias. Chem. Eur. J. 20: 11999 - 12003 (2014); https://doi.org/10.1002/chem.201403833

[29] Z. Zhao, Z. Yang, Y. Hu, J. Li, X. Fan, Appl. Surf. Sci. 476-481 (2013); https://doi.org/10.1016/j.apsusc.2013.03.119

[30] G. Bayramoglu, Arica, M. Yakup. Micropore mesopore mat. 226: 117-124 (2016); https://doi.org/10.1016/j.micromeso.2015.12.040

[31] Z. Raza Khan, M. Zulfequar, Mohd. Shahid Khan. Mater Sci Eng B Solid State Mater. 174: 145-149 (2010); https://doi.org/10.1016/j.mseb.2010.03.006

[32] R. Kumari, A. Sahai, N. Goswami, Prog. Nat. Sci.: Mater. Int. 25(4): 300-309 (2015); https://doi.org/10.1016/j.pnsc.2015.08.003

[33] D.G. Moon, S. Rehan, D.H. Yeon, S.M. Lee, S.J. Park, S. Ahn, Y.S. Cho, Sol. Energy Mater Sol. Cell. 200: 109963 (2019); https://doi.org/10.1016/j.solmat.2019.109963

[34] YH Ng, I.V. Lightcap, K. Goodwin, M. Matsumura, P.V. Kamat, J. Phys. Chem. Lett. 1: 2222-2227 (2010); https://doi.org/10.1021/jz100728z

[35] A. Balamurugan, M. Sudha, S. Surendhiran, R. Anandarasu, S. Ravikumar, YA Syed Khadar. Mater. Today: Proc. 26 3588-3594 (2020); https://doi.org/10.1016/j.matpr.2019.08.217

[36] C.N. Omprakash Anand, P. Thirunavukkarasu, S. Surendhiran, A. Balamurugan, K.C. Suresh, Y.A. Syed Khadar, AIP Conf. Proc. 2385: 020007 (2022); https://doi.org/10.1063/5.0070919

[37] Z. Li, F. Gong, G. Zhou, Z.S. Wang, J. Phys. Chem. C 117(13): 6561-6566 (2013); https://doi.org/10.1021/jp401032c

[38] J. Zhao, D. Xu, C. Gu, M.Y. Zhu, J. Huang, Mater. Chem. Phys. (2018); https://doi.org/10.1016/j.matchemphys.2018.06.072

[39] J. Jin, J. Yu, D. Guo, C. Cui, W. Ho, Small. 11(39): 5262-5271; https://doi.org/10.1002/smll.201500926

[40] Rajendra C. Pawar, V. Khare, C. Sunyong Lee, Dalton Trans. 43: 12514-12527 (2014); https://doi.org/10.1039/C4DT01278J

[41] N. Rajeswari Yogamalar, K. Sadhanandam, A. Chandra Bose, R. Jayavel, RSC Adv. 5: 16856-16869 (2015); https://doi.org/10.1039/C4RA13061H

[42] S. Karthikeyan, P. Thirunavukkarasu, S. Surendhiran, A. Balamurugan, Y.A. Syed Khadar, K. Shanmugasundaram, Mater. Today: Proc. 47(4) 964-969 (2021); https://doi.org/10.1016/j.matpr.2021.05.194

[43] H. Jin, L. Chen, A. Liu, L. Guan, D. Yin, P. Lin, S. Wang, W. Jiang, RSC Adv. 6: 28229-28235 (2016); https://doi.org/10.1039/C5RA27920H

[44] M. Ehtisham, K. Mohammad Mansoob Khan Moo Hwan Cho, J. Colloid Interface Sci. (2016); https://doi.org/10.1016/j.jcis.2016.07.070

[45] A. Kumar, Ramesh K. Sharma, N. Goyal, S. Gautam, Vacuum. (2018); https://doi.org/10.1016/j.vacuum.2018.10.018

[46] S. Sagadevan, K. Pal, Z. Zaman Chowdhury, J. Mater. Sci.: Mater. Electron. 28: 17193-17201 (2017); https://doi.org/10.1007/s10854-017-7648-1

[47] LL Li, K.P. Liu, G.H. Yang, C.M. Wang, J.R. Zhang, J.J. Zhu, Adv. Funct. Mater. 21: 869-878 (2011); https://doi.org/10.1002/adfm.201001550

[48] K. Pal, U.N. Maiti, T.P. Majumder, S.C. Debnath, Appl. Surf. Sci. 258: 163-168 (2011); https://doi.org/10.1016/j.apsusc.2011.08.024

[49] A.N. Cao, Z. Liu, S.S. Chu, M.H. Wu, Z.M. Ye, Z.W. Cai, Y.L. Chang, S.F. Wang, Q.H. Gong, Y.F. Liu, Adv. Mater. 22: 103-106 (2010); https://doi.org/10.1002/adma.200901920